Journal of Nuclear Materials 421 (2012) 9–14

Contents lists available at SciVerse ScienceDirect

Journal of Nuclear Materials

journal homepage: www.elsevier.com/locate/jnucmat

Review

In-situ SEM observation on the fracture of V–5Cr–5Ti alloy

Yufei Li [a,*], Ping Dong [a], Ruiwen Li [b], Jiangrong Yang [b], Jijia Xie [c]

[a] Science and Technology on Surface Physics and Chemistry Laboratory, P.O. Box 718-35, 621907 Mianyang, Sichuan, China
[b] China Academy of Engineering Physics, P.O. Box 919-71, 621900 Mianyang, Sichuan, China
[c] Institute of Mechanics, China Academy of Sciences, 100190 Beijing, China

ARTICLE INFO

Article history:
Received 11 January 2011
Accepted 10 November 2011
Available online 19 November 2011

ABSTRACT

The damage and fracture characteristic of V–5Cr–5Ti (wt.%) alloy was investigated using scanning electron microscope (SEM) with a micro-tension holder. Two types of specimen were used: smooth sheet and single-edge notched sheet. Results show that the microscopic fracture mechanism of smooth sheet alloy is microvoid coalescence and sliding off. What the fracture process shows is that the damage of smooth specimen stems from the inside. The alloy can be strengthened by single-edge notch but still remains considerable ductility. The main fracture mechanism of notched specimens is sliding off and quasi-cleavage. The main crack initiates at the root of notch and propagates along a zig-zag path. Grain boundary is a main barrier for crack propagation. Finite element method (FEM) simulation shows that the crack growth relaxes the stress of notched specimen, which in turn changes the fracture mechanism of alloy.

Contents

1. Introduction

V–(4–5)Cr–(4–5)Ti alloys have significant advantages for using as first wall and blanket structure materials in fusion devices [1–3]. Researchers have studied the fracture behavior and mechanism of V–5Cr–5Ti alloy. Results based on the fractography of quasi-static uniaxial tension showed that the alloys are typically ductile material with the microvoid coalescence fracture mechanism at ambient temperature [1–5]. The fracture mechanism and mechanical properties of V–Cr–Ti alloys can easily be changed [6–14]. For example, the fracture mechanism of compact tension (1/2 CT) specimens is different from the smooth uniaxial tensile specimens [3,8]. The crack growth direction along (*A*-direction) and perpendicular (*B*-direction) to the rolling orientation results in totally different fracture features. The *A*-direction fracture displays ductile tearing features and plastic deformation. On the other hand, the *B*-direction displays cleavage facets, intergranular secondary cracks and river patterns [8]. The V–5Cr–5Ti V-notch rectangular specimens, compared with the V–4Cr–4Ti, display a more brittle behavior; twinning, cleavage tongues, tearing steps and quasi-cleavage features manifest this [9]. Slip bands and short cracks also formed in the irradiated V–Cr–Ti alloy during tensile testing [6].

These studies on fracture behavior and mechanism mentioned above are based on the fractography after failure, but which cannot give more details about the fracture process. In the present paper, in situ SEM tensile testing were conducted to study the fracture

* Corresponding author.
E-mail address: liyufei034@yahoo.com.cn (Y. Li).

0022-3115/$ - see front matter © 2011 Elsevier B.V. All rights reserved.
doi:10.1016/j.jnucmat.2011.11.043

process and mechanism of V–5Cr–5Ti alloy under quasi-static uniaxial tension at ambient temperature.

2. Materials and experimental procedure

The V–5Cr–5Ti alloy used in this study was prepared by the following steps: double vacuum arc melting with self-consumable electrodes, hot-forging, rolling and finally annealing (1000 °C/1 h). Table 1 list the chemical composition of selected elements.

Fig. 1 shows the typical microstructures of the V–5Cr–5Ti alloy. The equiaxial grains and the Ti–CNO phases with band distribution appear in alloy after press working and annealing. Transmission electron microscopy observation shows that the diameter of the Ti–CNO phases is at the range of 30–50 nm. The yield strength, tensile strength, uniform elongation and area reduction of the alloy with gauge size ϕ 5 mm × 30 mm is 354 MPa, 460 MPa, 29% and 79%, respectively.

Several specimens were prepared by electrical discharge machining (EDM) along the rolling direction. Fig. 2 shows the geometry size of smooth specimens. Parts of the smooth specimen were cut by EDM at the middle to make a single-edge notch with radius of 0.1 mm and depth of 0.5 mm. All specimens were polished and etched using a solution of 20 vol.% HF + 20 vol.% HNO_3 + 60 vol.% H_2O. The average thickness of gauge after polishing is about 0.78 mm.

Tensile testing was performed on a Gatan microtest-2000 tensile stage attached to a FEI Sirion-400 SEM by controlling the displacement of the crosshead. All samples were tested at room temperature. At the beginning of testing, a stroke rate of 0.1 mm/min was adopted until the surface plastic deformation was observed, and then the rate was down to 0.033 mm/min until final fracture. Fracture of specimens were observed by SEM after tensile testing.

3. Results and discussion

3.1. The typically fracture process

Fig. 3 shows the fracture process of a smooth specimen in the in situ tensile testing. With the displacement increasing after yield, slip lines appear in some grains. Fig. 3a shows the surface features when necking appearing in width. Multiple slip and intersection slip in the bcc matrix also present. Likewise, slip bands was observed on the side surfaces of deformed tensile gauge section [6]. Fig. 3b shows the shape of the specimen just before final rupture. The necking in thickness leads to the surface subsidence. Increasing further load, the specimen suddenly rupture at the necking region (insert). No crack initiation and propagation is observed before rupture. This indicates that the damage of alloy stems from the inside. Fig. 3c shows the magnified features near the fracture. Grains are seriously elongated along the tensile direction and grain boundaries are undistinguishable. Some short transverse cracks (the arrows) initiate at grain boundaries but not propagate, which is similar to another experimental results [6].

Table 1
Average composition of V–5Cr–5Ti alloy.

Cr (wt.%)	Ti (wt.%)	C (μg/g)	O (μg/g)	N (μg/g)	Fe (μg/g)	Cu (μg/g)
5.2	4.9	55	380	76	<60	<20

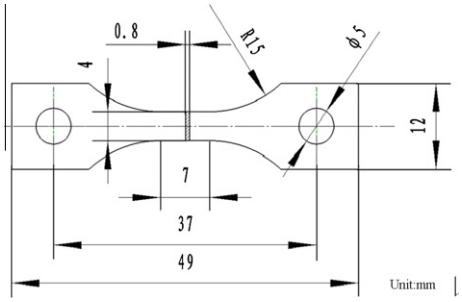

Fig. 2. Schematic dimensions of the smooth specimen.

3.2. In-situ observation on crack initiation and growth

To capture crack initiation and growth, single-edge notched specimens were adopted.

Fig. 4 shows the formation process of the main crack. The notch tip locates in a grain originally, as shown in Fig. 4a. Slip lines present step by step after the plastic deformation initiation. Increasing displacement, two transverse micro-cracks denoted as ***1***# and ***2***# initiate along the slip lines at the root of notch, as seen in Fig. 4b. That ascribes to the dehiscence of slip plans under normal stress [15,16]. Resume load, ***1***# crack become blunt ahead of a grain boundary, leading to strong non-uniform plastic deformation in grain ***Y*** (Fig. 4c). During loading further, ***1***# crack tears the grain boundary and propagates into grain ***Y***, as shown in Fig. 4d, and then the main crack forming. At the same time, some short microcracks appear but not propagate, as the arrows shown in Fig. 4d.

Fig. 5 shows the zig-zag propagation process of the main crack. The crack tip become blunt in the direction ***M*** firstly and then turns to the direction ***N*** which is nearly parallels to the slip lines, as seen

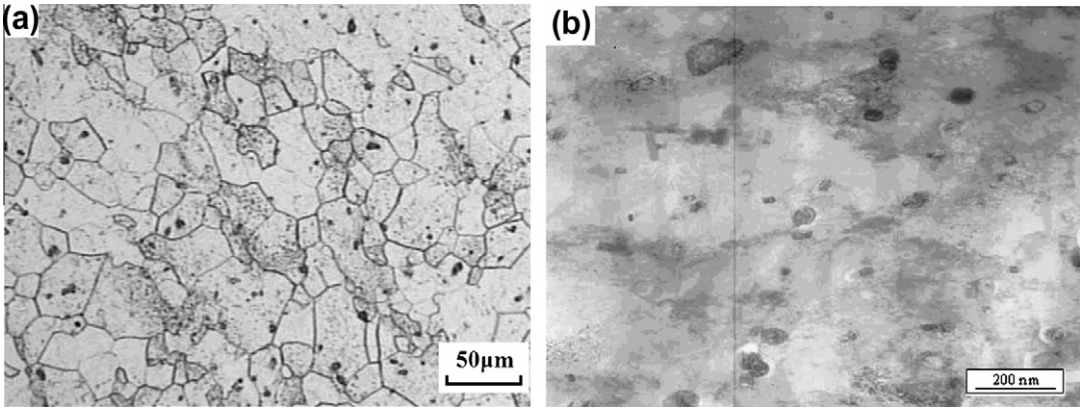

Fig. 1. Microstructures of V–5Cr–5Ti alloy. (a) Grain structures and (b) nano-size Ti–CNO phases.

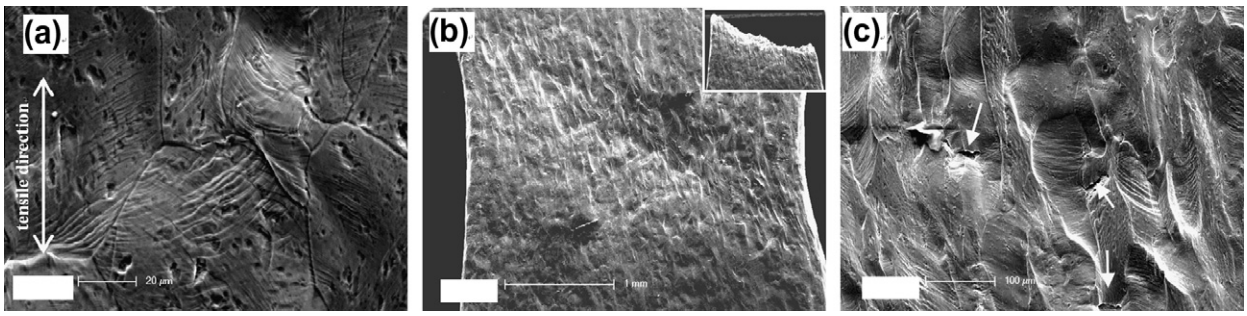

Fig. 3. The fracture process of V–5Cr–5Ti alloy. The insert in figure (b) is the feature of specimen after rupture. The microcracks are marked as arrows in figure (c).

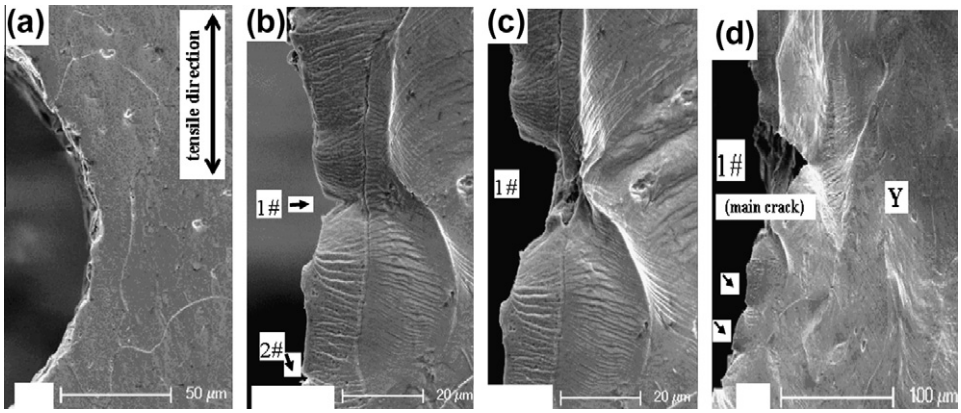

Fig. 4. The damage evolution and main crack formation of V–5Cr–5Ti alloy. Crack denoted as 1# is the main crack, denoted as 2# and other arrows are blunt cracks.

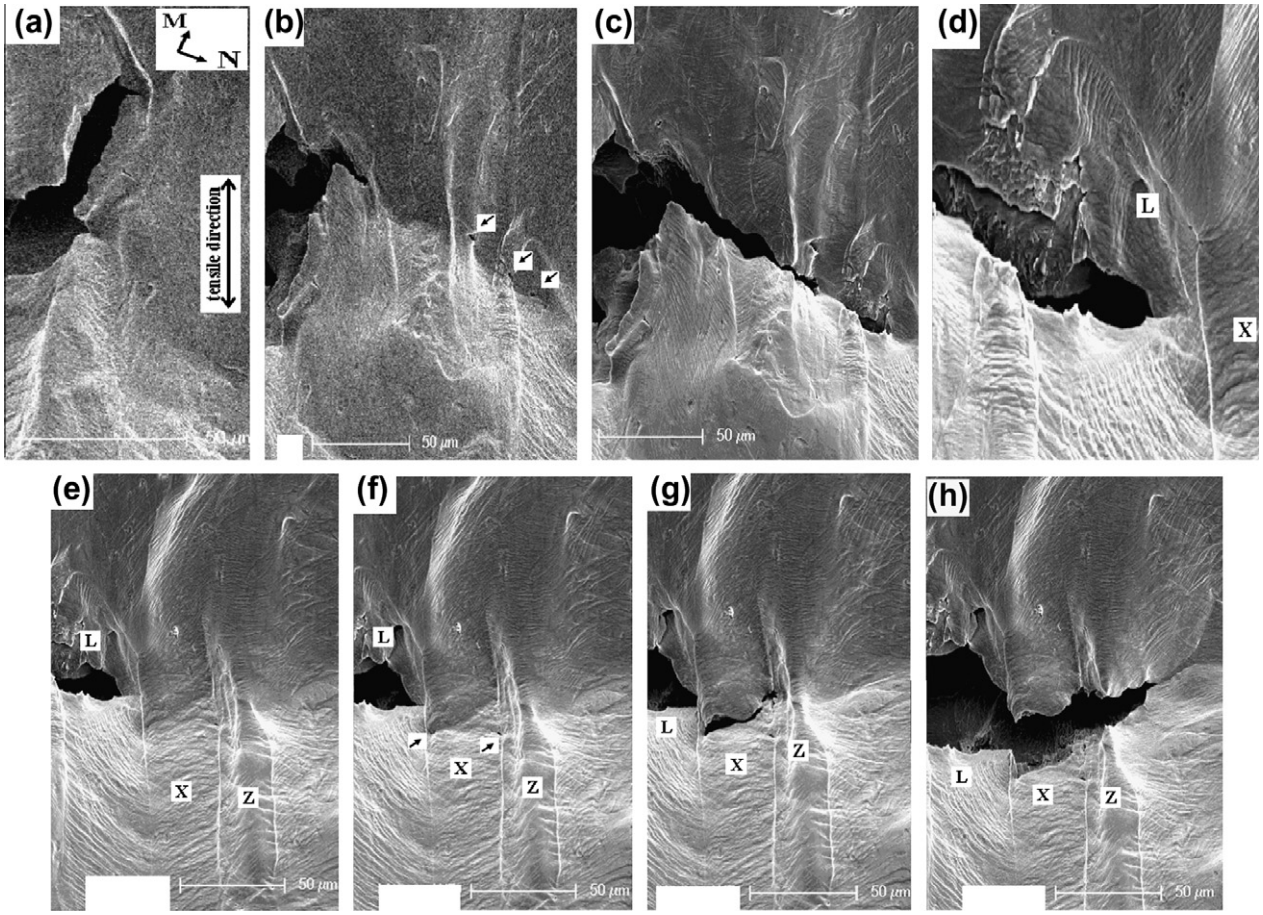

Fig. 5. Zig-zag growth of the main crack. Letter ***M*** and ***N*** denote the direction of crack propagation. Letter ***L***, ***X*** and ***Z*** denote grains. Regions marked as arrows are microvoids.

in Fig. 5a. With increasing displacement, the main crack propagates through two short zig-zag paths and some microvoids (the arrows) appear ahead of the crack tip synchronously, as shown in Fig. 5b. Then, the main crack propagates by merging the microvoids automatically during holding the displacement, as shown in Fig. 5c. Fig. 5d, which is the magnified details of the crack tip, shows that the propagation of the main crack is restrained by the boundary between grain ***L*** and ***X***.

With further extension, the main crack propagates about 6 μm toward the grain boundary and some voids initiate in grain ***X*** synchronously, as shown in Fig. 5e and Fig. 5f. Later, these voids in grain ***X*** incorporate each other to form a microcrack, which again leading to strongly plastic deformation in grain ***Z*** (Fig. 5g). Finally, the main crack propagate from grain ***L*** to grain ***Z*** through tearing the grain boundaries and merging the microcracks in grain ***X*** and grain ***Z***, as shown in Fig. 5h.

Fig. 6a shows the features of the main crack with 0.6 mm length. The crack opening displacement near the notch root is about 200 μm, which is equivalent to the original width of notch. Fig. 6b shows the features of specimen after final rupture. Deformation is mainly located in the region between the two dotted lines, indicating that the deformation of notched specimen is not uniform compared with smooth one.

3.3. Fracture mechanism

Fig. 7 shows the fracture features of two kinds of specimen. The fracture of smooth specimen are featured by dimples and discontinuously plastic holes, as shown in Fig. 7a. The wedge shape of plastic holes and the slip trace on the plastic holes are the typically features of sliding off mechanism. This mechanism, which is more popular in pure metal, is the result of the slip plane splitted by shear stress [16]. While in the dimples regions, there are many small equiaxed dimples with nano-size Ti–CNO phases (insert). The neck down of dimple walls leads to dimples coalescence. Measured and calculated from Figs. 7a and 3b, the area reduction of smooth one is about 65%.

Fig. 7b shows the fracture features of a notched specimen. The micro-fracture mechanism is a combination of microvoid coalescence, sliding off and more popular quasi-cleavage. The quasi-cleavage is seemly due to the three-dimensional stress ahead of the main crack tip. Looking back to Fig. 6a carefully, there are three regions marked as ***A***, ***B*** and ***C***. Surface subsidence presents in region ***A*** and ***B*** but absents in region ***C***. That is to say, the surface subsidence (i.e., necking in thickness) is just ahead of the main crack tip. The necking in thickness results in a three-dimensional stress distribution which restrains the plastic deformation of bulk material and then quasi-cleavage become domination. Aglan [9] also observed quasi-cleavage features in V–5Cr–5Ti V-notch tensile specimens. Calculated from Figs. 7b and 6b, the area reduction of notched specimen is about 50%.

That mixed fracture mechanism shown in Fig. 7 maybe ascribe to the non-uniform distribution of the nano-size Ti–CNO second phase, i.e., the bands in Fig. 1. Taking the smooth one for example, in the regions of second phase concentrated, the microvoid nucleation and coalescence mechanism is predominant; in the regions of second phase depleted, sliding off is the main mechanism. These big and deep plastic holes indicate a good plastic deformation ability of matrix [16]. While the fracture mechanism can easily be changed, such as the quasi-cleavage mechanism shown in Fig. 7b.

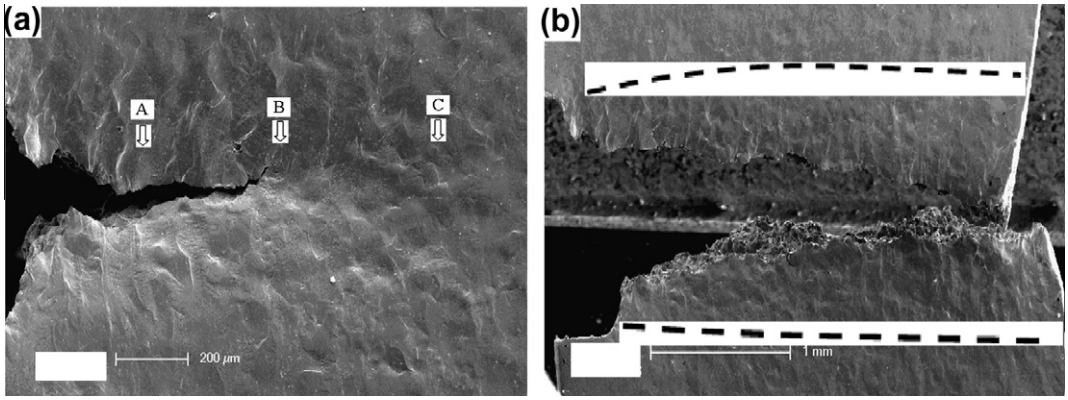

Fig. 6. The final rupture features of specimen. (a) The features of specimen during main crack propagation. The letter A–C represent three regions of specimen, which will be discussed in next section. (b) The final fracture features. The main deformation of specimen is concentrated in the region between dotted lines.

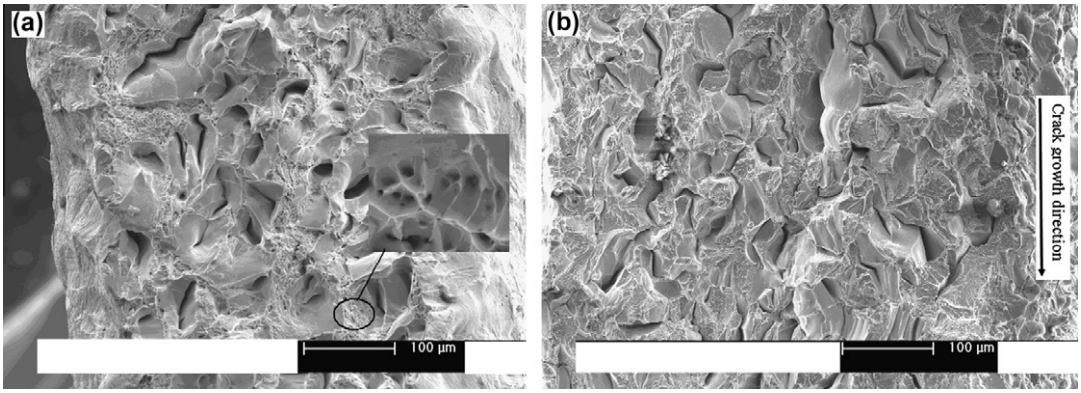

Fig. 7. Fractography of specimens. (a) The smooth one. The insert shows the nano-size particles at the bottom of dimples and (b) the notched one.

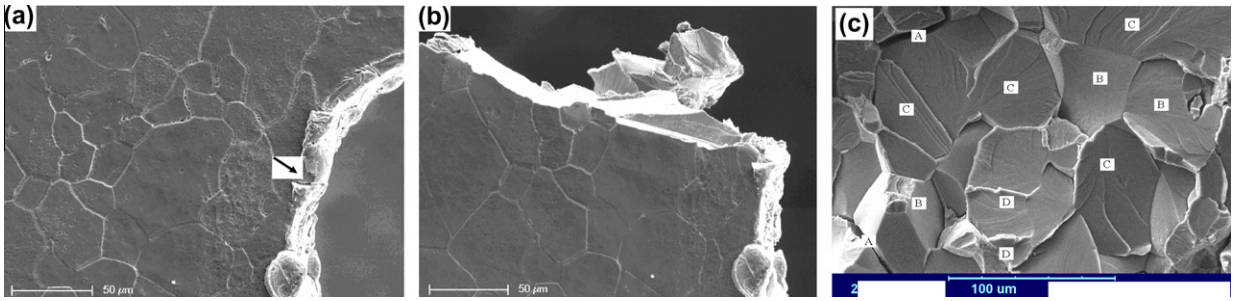

Fig. 8. Cleavage of V–5Cr–5Ti alloy. (a) Before testing. A small crack maybe exist in the arrowed zone which results in a totally cleavage of the specimen. (b) The features of the specimen after fracute. (c) The final fracture are featured by intergranular separation (at A), cleavage facets (at B), river patterns (at C) and twinning (at D).

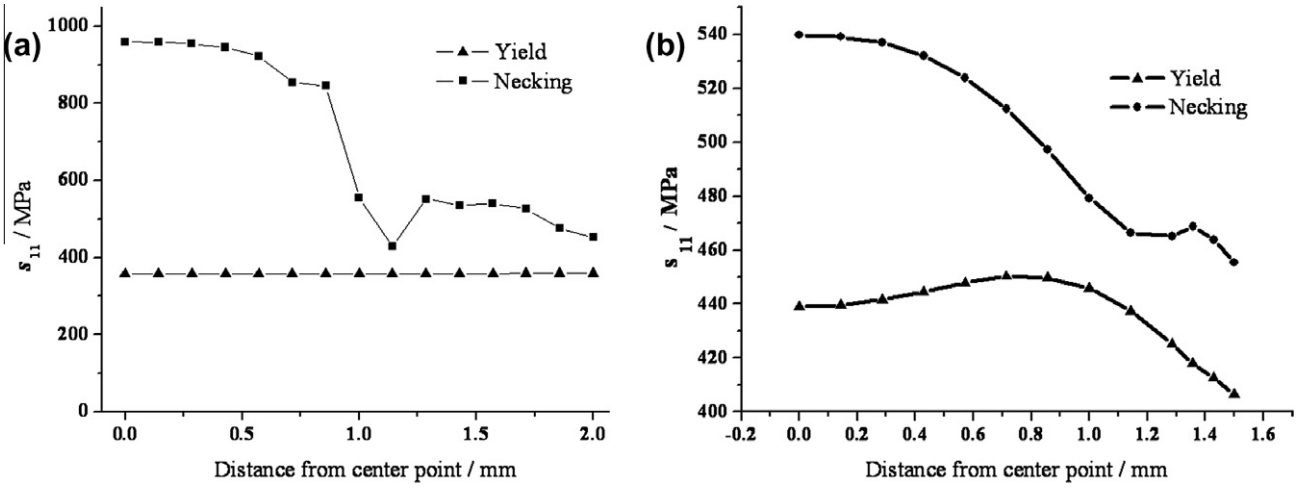

Fig. 9. Stress distribution of specimens at the beginning of yield and necking. (a) Without notch and (b) with notch.

Totally cleavage may also dominate in some special condition, as shown in Fig. 8. One of the notched specimens suddenly cleaves from the zone marked as a arrow in Fig. 8a. No evident plastic deformation is observed on the surface, as shown in Fig. 8b. The fracture are featured by intergranular separation (at A), cleavage facets (at B), river patterns (at C) and twinning (at D) in Fig. 8c, which are similar to other results [9]. Much smaller microcrack or twin, which is related to cleavage in BCC metal [9], maybe exist in the arrowed zone.

3.4. Mechanics analysis

Finite element method (FEM) was adopted to analyze the stress distribution of specimens at different deformation process. A quarter plane stress model was used because of the symmetry of specimens. The related input parameters for FEM simulation were revised by rod specimens firstly.

The stress distribution of two specimens from the center to the edge on the central cross-section at the beginning of yield and necking are shown in Fig. 9. At the beginning of yield, the stress of the smooth one is relatively uniform, which is comparable to the yield strength of the alloy (~354 MPa). While the overall stress of the notched one is higher compared with the smooth one, and there is stress concentration near the root of notch. Then, the area near the notch root will initiates plastic deformation before the bulk material. The experimental results demonstrated previous verified this.

Nevertheless, the stress distribution is different from each other at the beginning of necking, as seen in Fig. 9. For the smooth specimen, the stress on the center region is almost double than that at the edge region, which indicating that damage and microcrack will initiate at the center of the specimen firstly and then propagate to edge and surface. While for the notched one, the overall stress is much lower than the smooth one. This stress relaxation is due to the initiation and growth of crack near the root of notch. It is the different stress level after necking that leads to the different fracture mechanism for the two kinds of specimen. These simulation results are well consist with previously experimental results.

4. Conclusions

The smooth V–5Cr–5Ti sheet is a typically ductile material under quasi-static uniaxial tension. The plastic deformation is carried out by dislocation slip and grain boundary transformation. The microscopic tensile fracture mechanism is microvoid coalescence and sliding off. The fracture process and mechanism of alloy can be altered by outside notch. The main fracture mechanism of single U-type notched specimen is sliding off and quasi-cleavage. The main crack initiates at the root of notch and the microscopic propagation path is zig-zag. Grain boundary is a barrier for the propagation of crack.

5. Future works

The influence of some factors, such as notch size, tensile speed, grain size, on the crack initiation and propagation should be investigated in future. The grain orientation and (or) deformation twin

during plastic deformation should be studied by EBSD. The fracture process and micro-mechanism of bulk material should be investigated by in situ TEM tension.

Acknowledgements

This work was supported by the Science and Technology Foundation of CAEP under Grant No. 2009B0302036. Authors thanks Su Yang and Zhigang Wang for specimens preparation, and Tingting Liu for SEM analysis.

References

[1] A. Nishimura, A. Iwahori, N.J. Heo, T. Nagasaka, T. Muroga, S.-I. Tanaka, J. Nucl. Mater. 329–333 (2004) 438–441.
[2] D.T. Hoelzer, A.F. Rowcli, J. Nucl. Mater. 307–311 (2002) 596–600.
[3] A. Nishimura, T. Nagasaka, T. Muroga, J. Nucl. Mater. 307–311 (2002) 571–575.
[4] Huaxin Li, R.H. Jones, J.P. Hirth, Scr. Metall. Mater. 32 (4) (1995) 611–616.
[5] A.N. Tyumentsev, J. Nucl. Mater. 329–333 (2004) 429–433.
[6] H. Tsai, T.S. Bray, H. Matsui, M.L. Grossbeck, K. Fukumoto, J. Gazda, M.C. Billone, D.L. Smith, J. Nucl. Mater. 278 (2000) 362–366.
[7] H. Aglan, Y.X. Gan, B. Chin, M. Grossbeck, J. Nucl. Mater. 273 (1999) 192–202.
[8] H.A. Aglan, Mater. Lett. 62 (6–7) (2008) 865–869.
[9] H.A. Aglan, J. Nucl. Mater. 278 (2000) 186–194.
[10] V.A. Kazakov, V.P. Chakin, Yu D. Goncharenko, J. Nucl. Mater. 258–263 (1998) 1492–1496.
[11] M.L. Hamilton, M.B. Toloczko, J. Nucl. Mater. 283–287 (2000) 488–491.
[12] M. Satou, H. Koide, A. Hasegawa, J. Nucl. Mater. 233–237 (1996) 447–451.
[13] Jiming Chen, Shaoyu Qiu, Lin Yang, J. Nucl. Mater. 302 (2002) 135–142.
[14] K. Natesan, W.K. Soppe, J. Nucl. Mater. 233–237 (1996) 482–487.
[15] Liang Chunlei, Li xiaoyan, Gong shuili, Chen Li, Rare Met. Mater. Eng. 35 (2006) 1924–1927.
[16] Cui Yuexian, Wang Changli, Harbin Institute of Technology Press, P.R. China, 1998.